Advances in Colloid and Interface Science 245 (2017) 102–107

Contents lists available at ScienceDirect

Advances in Colloid and Interface Science

journal homepage: www.elsevier.com/locate/cis

Historical perspective

On the cohesion of fluids and their adhesion to solids: Young's equation at the atomic scale

J.-C. Fernandez-Toledano [a,*], T.D. Blake [a], P. Lambert [b], J. De Coninck [a]

[a] Laboratory of Surface and Interfacial Physics (LPSI), University of Mons, 7000 Mons, Belgium
[b] Université libre de Bruxelles, BEAMS CP165/56, Av. F.D. Roosevelt 50, B1050 Bruxelles, Belgium

ARTICLE INFO

Available online 21 March 2017

Keywords:
Wetting
Adhesion
Three-phase contact zone
Liquid-solid interface
Molecular-dynamics

ABSTRACT

Using large-scale molecular dynamics simulations, we model a 9.2 nm liquid bridge between two solid plates having a regular hexagonal lattice and analyse the forces acting at the various interfaces for a range of liquid-solid interactions. Our objective is to study the mechanical equilibrium of the system, especially that at the three-phase contact line. We confirm previous MD studies that have shown that the internal pressure inside the liquid is given precisely by the Laplace contribution and that the solid exerts a global force at the contact line in agreement with Young's equation, validating it down to the nanometre scale, which we quantify. In addition, we confirm that the force exerted by the liquid on the solid has the expected *normal* component equal to $\gamma_{lv}\sin\theta^0$, where γ_{lv} is the surface tension of the liquid and θ^0 is the equilibrium contact angle measured on the scale of the meniscus. Recent thermodynamic arguments predict that the *tangential* force exerted by the liquid on the solid should be equal to the work of adhesion expressed as $Wa^0 = \gamma_{lv}(1+\cos\theta^0)$. However, we find that this is true only when any layering of the liquid molecules close to liquid-solid interface is negligible. The force significantly exceeds this value when strong layering is present.

1. Introduction

As first described by Thomas Young [1] in his essay on cohesion of fluids in 1805, the competition between the cohesion of a fluid to itself and its adhesion to a solid gives rise to an angle of contact between the liquid and the solid that is specific to a given system at equilibrium. This conclusion leads to the necessary condition for mechanical equilibrium usually known as Young's equation. For a liquid on an ideal flat solid surface

$$\gamma_{lv}\cos\theta^0 = \gamma_{sv} - \gamma_{ls} \quad (1)$$

where θ^0 is the equilibrium contact angle and γ_{lv}, γ_{sv} and γ_{ls} are, respectively, the interfacial tensions between the liquid and the vapour, the solid and the vapour, and the liquid and the solid.

Although this equation has been thermodynamically validated [2,3] the quantities γ_{ls} and γ_{sv} are not generally accessible to experiment. But since, both γ_{lv} and θ^0 are easily measured, Eq. (1) is often used to determine the difference $\gamma_{sv}-\gamma_{ls}$. For a large class of interfaces, the thermodynamic approach has been confirmed from first principles on a microscopic basis using statistical mechanics [4–7] and also mechanically, through the continuum approximation where the interfaces are modelled as 2-D surfaces and the three-phase contact zone (TPZ), i.e. the intersection of a liquid–fluid interface with the liquid–solid interface, becomes a one-dimensional contact line. However, the mechanical interpretation of Young's equation, when treated as a force balance on the liquid and solid atoms present within the TPZ, is unclear at the near-molecular scale, as is the lower limit of the system size at which the equation is verified. Moreover, some recent papers have questioned the validity of Young's equation at this small scale [8,9].

In the light of this uncertainty and a desire to apply Young's equation in nanotechnology (for example to measure the forces of liquids on carbon fibres and nanocones [10,11]), several recent papers have been devoted to assessing the equation's validity at the nanoscale using molecular dynamics (MD). Their objective has been to understand the mechanical forces exerted by the liquid on the solid at this very small scale [12–15]. An additional thrust of this work has been to confirm the prediction [13] that the tangential force across the TPZ is equal to the thermodynamic work of adhesion expressed as $Wa^0 = \gamma_{lv}(1+\cos\theta^0)$ [12,13]. But, despite these efforts, the precise magnitude of this force remains in some doubt, as agreement with the computed forces was no better than 60–95%, depending on the value of θ^0 [13].

This was not the first time that MD had been used to study mechanical equilibrium at the contact line. Since the pioneering work of Saville in 1977 [16], the study of wetting by MD has advanced in line with computing power. Early, examples include the work of Sikkenk et al. [17] and Nijemeijer et al. [18], which were directed toward understanding wetting

* Corresponding author.
E-mail address: carlos.toledano@umons.ac.be (J.-C. Fernandez-Toledano).

http://dx.doi.org/10.1016/j.cis.2017.03.006
0001-8686/

and drying transitions. These were swiftly followed by investigations of two-liquid systems, e.g. Meyer et al. [19], Koplik et al. [20] and Thompson et al. [21]. The latter two studies involved moving contact lines, an important issue in its own right. Moving contact lines have also been the focus of more recent papers, e.g. de Ruijter et al. [22], Heine et al. [23], Seveno et al. [24], Bertrand et al. [25] and, most recently, Blake et al. [26] and Lukyanov and Likhtman [27]. In particular, this work sheds light on the vexed question of how a contact-line that moves can be reconciled with the standard no-slip condition between a liquid and a solid and whether or not the microscopic angle is velocity-dependent. Other important studies have focused on the magnitude and significance of line tension when the contact line is curved in the plane of the solid at a small scale [8,28,29]. Some of these questions have also been addressed by diffuse-interface/density-functional modelling (e.g. Refs [30,31].) and combined continuum-MD methods [32].

As discussed by Gibbs [2], Young's equation is thermodynamically validated for what he calls immutable solid, i.e. one sufficiently rigid to be unaffected by contact with the liquid. In the earliest investigation [16], the solid was assumed to be rigid but modelled as an external field rather than as an atomic solid. As the field progressed, the solid was treated either as a solid slab or as a crystalline lattice, with the atoms either in fixed positions or, more usually, tethered to the lattice by a strong harmonic potential, thus, minimising the risk that the solid supports a strain, which would modify its surface tension [33]. However, there has been at least one MD study of the consequences of a deformable substrate [13].

The objective of the study reported here is to use large-scale MD simulations to revisit the attractive forces between solids and liquids in contact down to the atomic scale. To do this, we analyze the force balance in a micro-channel: a liquid bridge confined between two parallel solid plates. We focus on the balance of forces at the TPZ for a range of equilibrium contact angles, not only from the perspective of the liquid, but also from that of the solid. The normal force exerted by the liquid on the solid, $\gamma_{lv}\sin\theta^0$, has already been verified by, for example, Ren and E [34]. The main way in which or study advances previous work is its focus on defining the TPZ at the atomic scale and accurately computing the tangential force exerted by the liquid on the solid in this region. In particular, we show that layering of the liquid adjacent to the solid wall leads to a tangential force at the contact line that exceeds $\gamma_{lv}(1+\cos\theta^0)$. A sound understanding of these effects is important in predicting the forces acting on nanomaterials at liquid interfaces.

Following the earlier work, we treat the solid as a tethered crystalline lattice, but allow the solid atoms to interact with each other with the same intensity as the liquid-liquid interactions. In common with most other studies, we do not determine the direct contribution of the solid surface tension to γ_{ls}, which is a potential source of error [18]. Rather, we compute the surfaces pressures π_{ls} exerted by the liquid at the solid surface. The surface pressure is the negative of what Gibbs [2] called the 'superficial tension' of the liquid in contact with the solid: $\pi_{ls} = -\varsigma_{ls} = \gamma_s - \gamma_{ls}$, where γ_s is the surface tension of the solid alone and constant. Using this concept, one may write Young's equation in the form $\gamma_l\cos\theta^0 = \pi_{ls} - \pi_{sv}$. If this force balance is validated, it implies that the solid is immutable at the level of simulation accuracy. To confirm this, we checked that moderate variations in the strength of the harmonic tethering potential did not affect our results.

2. Simulations

Full details of the simulation methods, base parameters and potentials have been given in our previous publications (e.g., Refs [26,27,35]. and work cited therein. We recall here the key aspects. The liquids, the solids and their interaction are modelled using Lenard-Jones potentials defined by:

$$V_{ij} = 4\varepsilon C_{AB}\left(\left(\sigma_{ij}/r_{ij}\right)^{12} - \left(\sigma_{ij}/r_{ij}\right)^{6}\right). \quad (2)$$

Here, r_{ij} is the distance between any pair of atoms i and j. The coupling parameter C_{AB} enables us to control the relative affinities between the different types of atoms. The parameters ε and σ are related, respectively, to the depth of the potential wells and an effective atomic diameter. For solid and liquid atoms $\sigma = 0.35$ and 0.25 nm, respectively, and $\varepsilon = k_BT$ where k_B is the Boltzmann constant and $T = 33$ K is the temperature, which is kept constant by a thermostat based on velocity scaling. The pair potential is set to zero for $r_{ij} > 2.5\sigma$. C_{AB} is given the value 1 for both liquid–liquid (L–L) and solid–solid (S—S) interactions, but for the solid–liquid (S–L) interaction it is varied from 0.2 to 0.6 to explore a wide range of equilibrium contact angles (from approximately 147° to 46°, respectively). The masses of all the atoms are equated to that of carbon to allow comparison with physical systems. The main parameters and macroscopic quantities employed in the simulations are listed in Table 1.

The solid plates are constructed as regular hexagonal lattices having three atomic layers. To maintain rigidity, while permitting exchange of momentum with the liquid, the solid atoms are allowed to vibrate thermally around their initial positions by a strong harmonic potential. The liquid is modelled as 5608 8-atom molecular chains, with adjacent atoms linked by a confining potential $V_{conf} = \varepsilon r_{ij}^6/\sigma^6$. This minimizes evaporation over the time scale of the simulation, so that the vapour phase is effectively a vacuum. The dimensions of the simulation box are L_x, L_y, $L_z = 42.9$, 8.4 and 11.3 nm, respectively, and we impose periodical boundary conditions in the x and y directions. The two parallel plates, each comprising 14,535 atoms, are located in the extremities of the z-axis. We fix the distance between the plates $H = 9.2$ nm. Fig. 1 shows a snapshot of the system for $C_{SL} = 0.2$.

At the start of each simulation, the liquid is equilibrated between the two plates for up to 1.5×10^6 time steps (7.5 ns), as indicated by a contact angle that fluctuates around a stationary value. To determine this angle, the positions of the front and back menisci are first located by a density calculation, choosing the location to be where the density falls to 50% of the bulk (the equimolar surface). The equilibrium contact angle is then found by fitting an arc of a circle to the bulk profile away from the contact line and measuring its tangent at the solid, as in a real experiment. More details of this procedure can be found in Ref. [35]. The time step between computational iterations is 5 fs.

3. Forces on the liquid

To analyze the force balance across the whole liquid, we calculate the local pressure at each point according to the method proposed in Ref. [36]. The total pressure is the sum of two contributions: that due to the pair-wise interactions and the kinetic component due to the momentum of the liquid molecules. The pressure is a second-order tensor $\boldsymbol{P}$, where the component $P^{\alpha\beta}$ gives the force per unit area in the β-direction across a surface pointing in the α-direction. We define P^{xx} and P^{zz} as the tangential and normal components of the pressure tensor with respect to the solid surface. Since the solid surface is flat, the normal pressure will be the same within the solid and the liquid, with a value equal to the isotropic pressure of the bulk liquid, $P^{zz} = P_B$, which we compute

Table 1
Parameters associated with the simulations carried out in this work. σ_{LL} and σ_{LL} are the diameters of the liquid and solid atoms, respectively; T is the temperature, ε is related to the depth of the Lennard-Jones potential well, γ_{lv} is the surface tension, η is the viscosity, ρ_0 is the density of the liquid, r_c is the Lennard-Jones cut–off, m_0 is the mass of the liquid atom, and C_{LL}, C_{SS} and C_{SL} are the liquid–liquid, solid–solid and solid-liquid coupling parameters.

Magnitude	Value	Magnitude	Value
σ_{LL}	0.35 nm	ρ_0	18.26 atoms/nm^3
σ_{LS} (nm)	0.25 nm	r_c	0.875 nm
T (K)	33 K	m_0	12 g/mol
ε	277 J/mol	C_{LL}	1
γ_{lv}	2.49 mN/m	C_{SS}	1
η	0.248 mPa·s	C_{SL}	0.2, 0.3, 0.35, 0.4, 0.45, 0.5, 0.55, 0.6

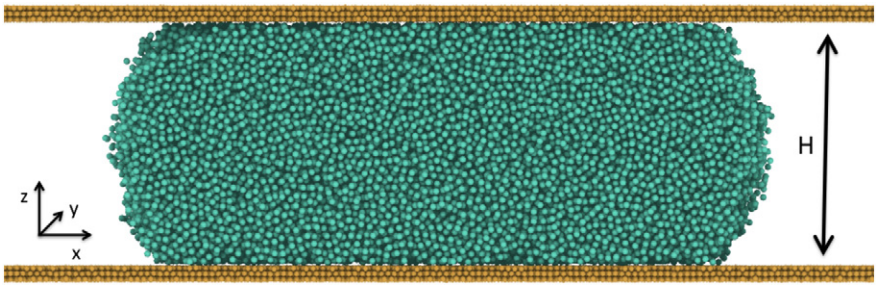

Fig. 1. Snapshot of the system at equilibrium for $C_{SL} = 0.2$.

using the Irving and Kirkwood method [37]. Hence, the normal forces acting on the liquid and the solid at the TPZ will have the same value but opposite sign. The tangential pressure in the liquid can be decomposed into three different contributions: the liquid–liquid, P^{xx}_{LL}, solid–liquid, P^{xx}_{SL}, and the thermal, $k_BT\rho_L$:

$$P^{xx}(xz) = P^{xx}_{LL}(xz) + P^{xx}_{SL}(xz) + k_BT\rho_L(xz) \tag{3}$$

where $\rho_L(x,z)$ denotes the density of the liquid in the x,z plane.

Due to the substitution of the liquid atoms by solid at the solid–liquid interface, there is an anisotropy between the tangential and normal components of the pressure tensor close to this interface. This induces a non-zero surface pressure that can be expressed as:

$$\pi_{ls}(x) = \int_{\Delta L} (P^{zz} - P^{xx}(xz))dz \tag{4}$$

where, ΔL represents the thickness of the liquid–solid interface. The homogeneity of the solid means that any liquid atom of the system located at x will interact with the same number of solid atoms in region $x + \delta$ as in $x - \delta$. Therefore, the net tangential force induced by the solid on any the liquid atom will be zero. This symmetry will also hold at the TPZ, so introducing Eq. (3) in Eq. (4) and eliminating the liquid–solid contribution $P^{xx}_{SL}(x,z)$ we have:

$$\begin{aligned}\pi_{ls}(x) &= \int_0^{H/2} (P^{zz} - (P^{xx}(x,z) - P^{xx}_{SL}(x,z))dz \\ &= \int_0^{H/2} (P^{zz} - P^{xx}_{LL}(x,z) - k_BT\rho_L(x,z))dz\end{aligned} \tag{5}$$

This surface pressure is constant at the general S–L interface, but decays to zero across each TPZ. Therefore, the net force due to the gradient of pressure in these marginal regions is $F^x_{TPZ} = -\pi_{ls}(x)$. This is compensated by the tangential force exerted by the L–V interface at the contact line, which, according to Young's equation, should be equal to $\gamma_{lv}\cos\theta^0$. Thus, we expect

$$F^x_{TPZ} = -\pi_{ls}(x) = \gamma_{lv}\cos\theta^0. \tag{6}$$

To compute the surface pressures from Eq. (5), we first determine the liquid-liquid contribution to the tangential pressure $P^{xx}_{LL}(x,z)$ within the liquid L. We place a virtual plane perpendicular to the x axis at the centre of the L_i–S interface x_k. This splits L into two subsystems: the left containing atoms in the interval $x_i \in [x_k - r_c, x_k]$, and the right containing atoms in the interval $x_i \in [x_k, x_k + r_c]$. The left subsystem is then sliced into parallel layers of thickness $dz = 0.2$ nm, and from the derivative of the Lenard-Jones potential, Eq. (2), we calculate the force f_{LJ} acting on the liquid atoms within each layer due to the liquid atoms to the right of the plane at x_k:

$$P^{xx}_{LL}(x_k, z_l) = \frac{1}{L_y dz}\sum_{i=1}^{N_L}\sum_{j=1}^{N_L} f^x_{LJ}(r_{ij})\Theta(x_i - x_k)\Theta(x_k - x_j)\delta_{il} \tag{7}$$

Here, $f^x_{LJ}(r_{ij})$ is the x component of the Lennard-Jones force between liquid atoms i and j, N_L the number of liquid atoms and L_y the y dimension of the simulation box. The Heaviside step function $\Theta(x)$ is used to ensure we consider only atoms located in the separate subsystems on either side of the plane at x_k; and δ_{il} takes the value 1 if atom i is located in layer z_l or 0 in any other case to ensure we associate the force with the appropriate layer. Then, knowing P^{xx}_{LL} from Eq. (7), ρ_L and P_B, we can compute the surface pressures inside the liquid using Eq. (5) and so check the force balance predicted by Eq. (6).

Fig. 2 illustrates the excellent agreement achieved. Here, the surface tension of the liquid, $\gamma_{lv} = 2.49 \pm 0.5$ mN/m, was calculated using a standard method [35] in an independent simulation with a planar liquid film. The data represent the averaged results of 1000 configurations and the error bars the standard deviations of the averages. Note that the solid does not directly contribute to the tangential pressure in the liquid. Any liquid atom located at some position x will interact with the same number of solid atoms at $x - \delta$ as at $x + \delta$; thus, the net tangential force induced by the solid at this position will be zero. This symmetry will also hold across the TPZ.

4. Forces on the solid

To determine the forces on the solid, we first compute the forces acting on each solid atom from the liquid. Due to the symmetry of the system in the y direction, the solid atoms may then be projected onto the x–z plane, which we subdivide into a grid with $dx = 0.4$ nm and dz equal to the three atomic layers of the solid plate. For each cell C_k of the grid, located at x_k, we define $\vec{F}_{LS}(x_k)$ as the total force per unit length of the contact line exerted by liquid L on the solid atoms inside cell C_k:

$$\begin{aligned}\vec{F}_{LS}(x_k) &= \frac{1}{L_y}\sum_{i=1}^{N_S}\sum_{j=1}^{N_L}\vec{f}^{LJ}(r_{ij})\delta_{ik} \\ &= F^x_{LS}\hat{x} + F^z_{LS}\hat{z}\end{aligned} \tag{8}$$

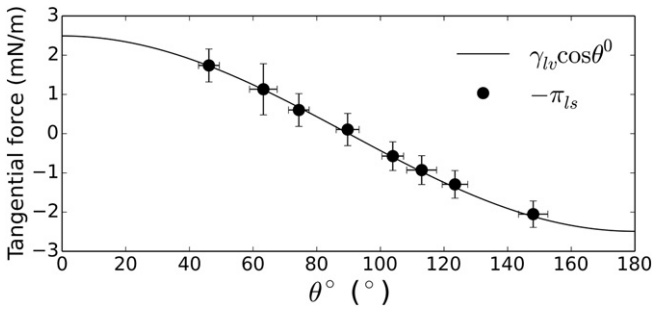

Fig. 2. Result of integrating Eq. (4) at the solid-liquid interface compared with $\gamma_{lv}\cos\theta^0$.

where $\delta_{ik} = 1$ if the solid atom i belongs to cell C_k or 0 if not. L_y is the y dimension of the simulation box corresponding to the length of the contact line, and F^z_{LS} and F^x_{LS} represent, respectively, the normal and tangential forces (with respect to the solid–liquid interface) exerted by the liquid on the solid inside the cell C_k. We then average these force profiles over 1000 configurations to produce the complete distribution of forces along each solid plate.

Fig. 3 shows examples of the tangential and normal force profiles acting on the bottom solid plate due to the presence of the liquid. The peaks in each profile correspond to the locations of the TPZ, which are corroborated by the decay in the density and the pressure profiles. The normal force profiles acting on the bottom wall for couplings $C_{SL} = 0.2$, 0.45 and 0.6 are shown in Fig. 3a and correspond to equilibrium contact angles of 147°, 90° and 46°, respectively. The positive values of the peaks are associated with a force pointing into the liquid and, therefore, to the attraction of the solid plate by the liquid. In the intervening central region, the profiles settle to a constant plateau value. Since the pressure outside the liquid is zero (a vacuum), the normal pressure at the centre of the S–L interface, P_c should be equal simply to the Laplace pressure $P_c = \Delta P = 2\gamma_{lv}/H\cos\theta^0$. Fig. 4 confirms that the agreement between the two is very good, which validates the methods we have used to compute the forces acting on the solid.

Another conclusion that can be drawn from these calculations is the scale below which it would be inappropriate to apply Young's equation. In Eq. (1) the various surface tensions are macroscopically measureable quantities and the TPZ is modelled as a one-dimensional contact line. Fig. 3 shows that in the simulations this line is in fact a zone of width 3.7 ± 0.23 nm computed as the length of the intersection between the fitted Gaussian function to each peak of the tangential force and the horizontal line $y = \Delta F_c$ where ΔF_c is the standard deviation of the tangential force at the centre of the solid-liquid interface. This is greater than the thickness of the liquid meniscus (about 2.2 nm) and becomes significant if the liquid-solid contact region approaches the same scale. Below this scale, therefore, deviations from (1) are to be expected.

Within the TPZ, the total normal force has two contributions: the Laplace pressure and the component due to the L–V interface. The Laplace pressure must disappear at the contact line. Since intermolecular forces depend on the number of interacting atoms, a reasonable approach is to assume that the pressure decays with liquid density profile $\rho(x)$ across the TPZ: $\Delta P(x) = P_c\rho(x)/\rho_0$, where ρ_0 is the density in the bulk. The contribution of the L–V interface to the normal force at the contact line is then given by the integral of $P^{xx}(x) - \Delta P(x)$, which, according to Young's equation, should be equal to $\gamma_{lv}\sin\theta^0$:

$$F^z_{TPZ} = \int_{TPZ} (P^{zz}(x) - \Delta P(x))dx = \gamma \sin\theta^0 \tag{9}$$

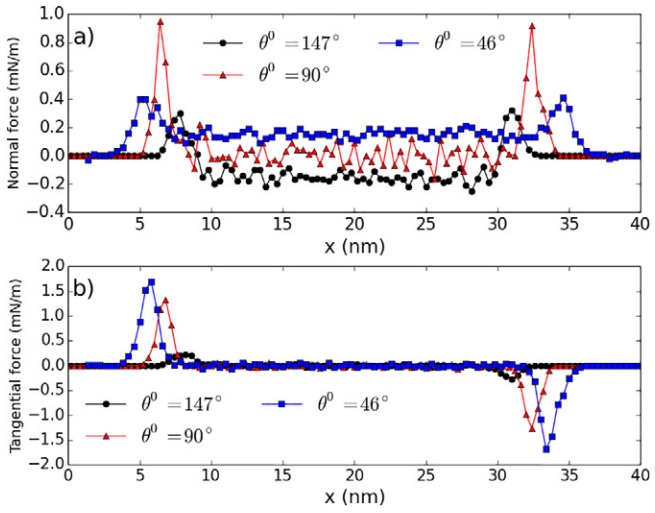

Fig. 3. (a) Normal force profiles for different C_{SL} and θ^0. (b) Tangential force profile for different C_{SL} and θ^0. Both plots correspond to the forces acting on the bottom plate.

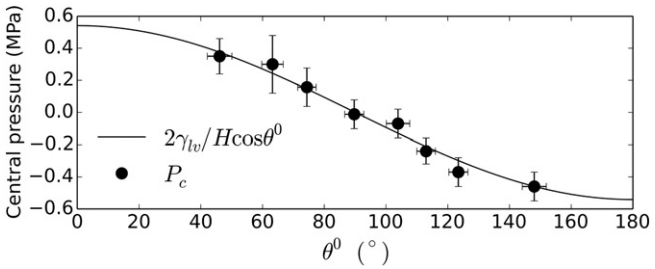

Fig. 4. The pressure P_c measured at the centre of the S–L interface versus θ^0 compared with the expected value of the Laplace pressure. The data are the average values obtained from 1000 configurations over the whole of the bulk liquid. The error bars are the standard deviations of the averages.

Fig. 5a shows that the computed normal force at the contact line, plotted as a function of the equilibrium contact angle, is in very good agreement with the expected value.

The sum of the points belonging to the peaks of the tangential force profiles (e.g., that plotted in Fig. 3b) gives the total tangential force at the TPZ, and the sign of the peaks reveals that the force is pointing inward, toward the liquid. The sum of the full tangential profile is equal to zero, which is consistent with equilibrium. Recently, a model for the tangential force of the liquid on the solid has been proposed based on density functional theory [14]. According to the arguments presented, the force should be $\gamma_{lv}(1 + \cos\theta^0)$, i.e. the equilibrium work of adhesion Wa^0, defined as the energy required to destroy unit area of S–L interface and create equivalent areas of S–V and L–V interface at constant temperature and pressure. This prediction has been corroborated by computer simulations [12,13] and some supporting experimental evidence [38]. That the force is not simply $\gamma_{lv}\cos\theta^0$ is due to the absence of liquid on the vapour side of the interface; hence, the attraction is always

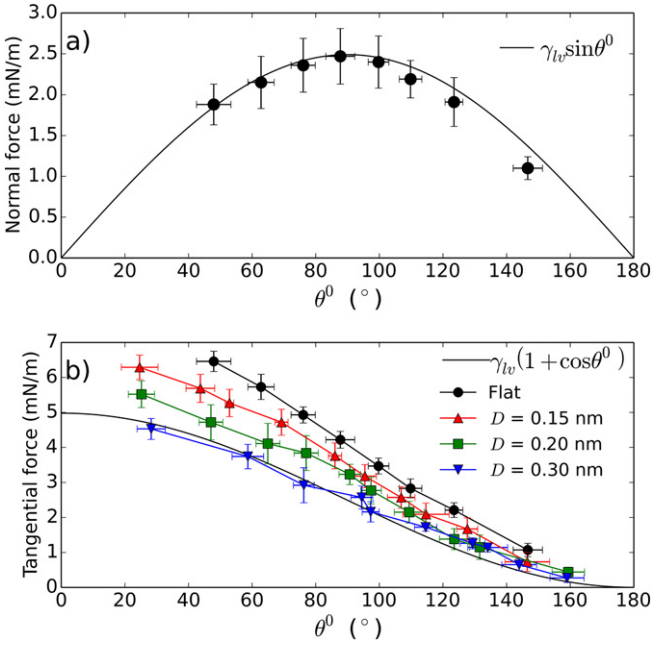

Fig. 5. (a) Total normal force of the liquid on the solid at the contact line compared with $\gamma_{lv}\sin\theta^0$. (b) Total tangential force acting at the contact line for different levels of solid roughness, D, compared with $\gamma_{lv}(1 + \cos\theta^0)$.

positive in the direction of the liquid and, therefore, equal to the work of adhesion. From the perspective of the liquid, the solid is continuous in both directions about the contact line, so the force must change sign when the angle is 90° and so follow $\gamma_{lv}\cos\theta^0$ [15].

Fig. 5b shows the total tangential force of the liquid on the solid computed from our simulations. As before the data are the averages of 1000 configurations and the error bars are associated standard deviations. The upper data set (labelled 'flat') is the result obtained with the solid constructed as described earlier. While it is clear that the results are in qualitative agreement with expectation, the forces are significantly larger than predicted. Similar problems have been reported by others: e.g., Fig. 2 in Ref. [13]. Given that we successfully compute the normal forces at the contact line, why then do similar methods lead to an apparent overestimate of the tangential forces?

We propose that the key to understanding this discrepancy is the molecularly flat, layered lattice used to model the solid. This structure induces a strong layering in the liquid close to the S-L interface, as shown for example in Fig. 6 for $C_{SL} = 0.45$, which mirrors that in the solid. Since the forces depend on the densities of the interacting phases, the layering directly affects the calculations. This effect was addressed by Navascués and Berry [39], who argued that the thermodynamic work of adhesion for a liquid being separated from a solid consists of two terms: one that depends on the S–L interaction and is the work necessary to remove the liquid from the solid without modifying its density profile. The other is the energy released when the density distribution relaxes to equilibrium profile for a liquid with a free surface. The stronger the layering the greater will be the effect of this entropic term.

To check this idea, we randomly select 50% of the solid atoms belonging to the layer of the plates closest to the liquid phase and vary the distance between them and the liquid molecules by a random length $\zeta \in [0, D]$ where $D = 0.15$, 0.2 and 0.3 nm. Fig. 6 shows the drastic reduction in liquid layering as D is increased for $\theta^0 = 90^\circ$. The associated tangential forces are showed in Fig. 5b, where it can be seen clearly that they approach $\gamma_{lv}(1 + \cos\theta^0)$ as liquid layering is reduced. We believe the neglect of this effect may have lead to the discrepancies seen in earlier work [13]. The fact that Seveno et al. [12] achieved better agreement is probably due to reduced layering around the highly curved nanofibre modelled in the simulations and the use of an effective radius (necessitated by the cubic lattice of the solid) to calculate the force per unit length at the contact line.

5. Conclusions

By recovering $\gamma_{lv}\cos\theta^0$ and $\gamma_{lv}\sin\theta^0$ for, respectively, the tangential and normal forces acting at the contact line, our large-scale MD simulations have confirmed the validity of the Young's equation at the nanoscale down to the width of the three-phase zone, i.e. 3.7 ± 0.23 nm in our simulations. Below this scale deviations are to be expected. The normal pressure of the liquid has also been determined and shown to be equal to the Laplace pressure; thus validating our methods. Finally, the tangential force exerted by the liquid on the solid at the contact line has been measured as a function of solid-liquid interactions and found to be greater than the work of adhesion expressed as $\gamma_{lv}(1 + \cos\theta^0)$. By introducing a small random roughness in the solid surface, we have confirmed that this effect is due to the layering of the liquid in contact with an ordered solid. The roughness eliminates the layering and enables us to recover $\gamma_{lv}(1 + \cos\theta^0)$. While we can readily identify the solid-liquid interface in our simulations, with many practical systems the solid surface is rough at the atomic-scale and the solid-liquid interface is diffuse and ill-defined. Thus, the issue of layering, while of fundamental importance in understanding Young's equation, may be less critical in every-day applications.

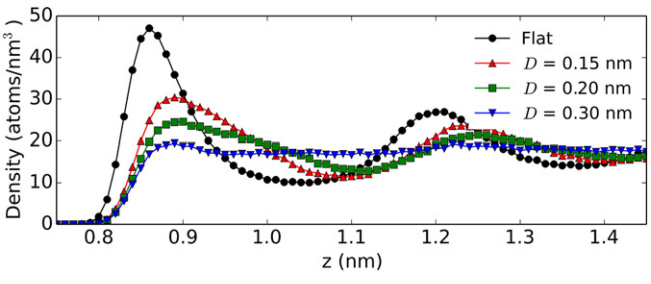

Fig. 6. The liquid density profile in the z direction at the centre of the S-L interface for $C_{SL} = 0.45$ showing the reduction in layering with increasing solid roughness D.

Acknowledgements

This research was partially funded by the Interuniversity Attraction Poles Programme (IAP 7/38 MicroMAST) of the Belgian Science Policy Office.

References

[1] Young T. An essay on the cohesion of fluids. Philos Trans R Soc London 1805;95:65–87. http://dx.doi.org/10.1098/rstl.1805.0005.
[2] Gibbs JW. Collected works. , 1New York: Longmans, Green; 1928. http://dx.doi.org/10.1109/JSSC.2006.874331.
[3] Johnson RE. Conflicts between Gibbsian thermodynamics and recent treatments of interfacial energies in solid-liquid-vapor. J Phys Chem 1959;63:1655–8. http://dx.doi.org/10.1021/j150580a021.
[4] De Coninck J, Dunlop F. Partial to complete wetting: a microscopic derivation of the Young relation. J Stat Phys 1987;47:827–49. http://dx.doi.org/10.1007/BF01206160.
[5] De Coninck J, Dunlop F, Rivasseau V. On the microscopic validity of the Wulff construction and of the generalized Young equation. Commun Math Phys 1989;121:401–19. http://dx.doi.org/10.1007/BF01217731.
[6] Abraham D, Ko L. Exact derivation of the modified Young equation for partial wetting. Phys Rev Lett 1989;63:275–8. http://dx.doi.org/10.1103/PhysRevLett.63.275.
[7] Deuschel J-D, Giacomin G, Ioffe D. Large deviations and concentration properties for $\nabla\phi$ interface models. Probab Theory Relat Fields 2000;117:49–111. http://dx.doi.org/10.1007/s004400050266.
[8] Ingebrigtsen T, Toxvaerd S. Contact angles of Lennard-Jones liquids and droplets on planar surfaces. J Phys Chem C 2007;111:8518–23. http://dx.doi.org/10.1021/jp0676235.
[9] Makkonen L. Young's equation revisited. J Phys Condens Matter 2016;28:135001. http://dx.doi.org/10.1088/0953-8984/28/13/135001.
[10] Barber AH, Cohen SR, Wagner HD. Static and dynamic wetting measurements of single carbon nanotubes. Phys Rev Lett 2004;92:186103. http://dx.doi.org/10.1103/PhysRevLett.92.186103.
[11] Delmas M, Monthioux M, Ondarçuhu T. Contact angle hysteresis at the nanometer scale. Phys Rev Lett 2011;106:136102. http://dx.doi.org/10.1103/PhysRevLett.106.136102.
[12] Seveno D, Blake TD, De Coninck J. Young's equation at the nanoscale. Phys Rev Lett 2013;111:1–4. http://dx.doi.org/10.1103/PhysRevLett.111.096101.
[13] Weijs JH, Andreotti B, Snoeijer JH. Elasto-capillarity at the nanoscale: on the coupling between elasticity and surface energy in soft solids. Soft Matter 2013;9:8494. http://dx.doi.org/10.1039/c3sm50861g.
[14] Das S, Marchand A, Andreotti B, Snoeijer JH. Elastic deformation due to tangential capillary forces. Phys Fluids 2011;23:72006. http://dx.doi.org/10.1063/1.3615640.
[15] Marchand A, Weijs JH, Snoeijer JH, Andreotti B. Why is surface tension a force parallel to the interface? Am J Phys 2011;79:999. http://dx.doi.org/10.1119/1.3619866.
[16] Saville G. Computer simulation of the liquid–solid–vapour contact angle. J Chem Soc, Faraday Trans 2 1977;73:1122–32. http://dx.doi.org/10.1039/F29777301122.
[17] Sikkenk JH, Indekeu JO, van Leeuwen JMJ, Vossnack EO, Bakker AF. Simulation of wetting and drying at solid-fluid interfaces on the Delft Molecular Dynamics Processor. J Stat Phys 1988;52:23–44. http://dx.doi.org/10.1007/BF01016402.
[18] Nijmeijer MJP, Bruin C, Bakker AF, van Leeuwen JMJ. Wetting and drying of an inert wall by a fluid in a molecular-dynamics simulation. Phys Rev A 1990;42:6052–9. http://dx.doi.org/10.1103/PhysRevA.42.6052.
[19] Meyer M, Mareschal M, Hayoun M. Computer modeling of a liquid–liquid interface. J Chem Phys 1988;89:1067–73. http://dx.doi.org/10.1063/1.455259.
[20] Koplik J, Banavar JR, Willemsen JF. Molecular dynamics of fluid flow at solid surfaces. Phys Fluids A Fluid Dyn 1989;1:781–94. http://dx.doi.org/10.1063/1.857376.
[21] Thompson PA, Brinckerhoff WB, Robbins MO. Microscopic studies of static and dynamic contact angles. J Adhes Sci Technol 1993;7:535–54. http://dx.doi.org/10.1163/156856193X00844.
[22] de Ruijter MJ, Blake TD, De Coninck J. Dynamic wetting studied by molecular modeling simulations of droplet spreading. Langmuir 1999;15:7836–47. http://dx.doi.org/10.1021/la9901711.
[23] Heine DR, Grest GS, Webb EB. Spreading dynamics of polymer nanodroplets. Phys Rev E 2003;68:61603. http://dx.doi.org/10.1103/PhysRevE.68.061603.
[24] Seveno D, Ogonowski G, De Coninck J. Liquid Coating of Moving Fiber at the Nanoscale; 2004. http://dx.doi.org/10.1021/LA049574Y.
[25] Bertrand E, Blake TD, De Coninck J. Influence of solid–liquid interactions on dynamic wetting: a molecular dynamics study. J Phys Condens Matter 2009;21:464124. http://dx.doi.org/10.1088/0953-8984/21/46/464124.

[26] Blake TD, Fernandez-Toledano J-C, Doyen G, De Coninck J. Forced wetting and hydrodynamic assist. Phys Fluids 2015;27:112101. http://dx.doi.org/10.1063/1.4934703.
[27] Lukyanov AV, Likhtman AE. Dynamic contact angle at the nanoscale: a unified view. ACS Nano 2016;10:6045–53. http://dx.doi.org/10.1021/acsnano.6b01630.
[28] Bresme F, Quirke N. Nanoparticulates at liquid/liquid interfaces. Phys Chem Chem Phys 1999;1:2149–55. http://dx.doi.org/10.1039/a901006h.
[29] Peng H, Birkett GR, Nguyen AV. The impact of line tension on the contact angle of nanodroplets. Mol Simul 2014;40:934–41. http://dx.doi.org/10.1080/08927022.2013.828210.
[30] van Swol F, Henderson JR. Wetting and drying transitions at a fluid-wall interface. Density-functional theory versus computer simulation. II. Phys Rev A 1991;43:2932–42. http://dx.doi.org/10.1103/PhysRevA.43.2932.
[31] Herring AR, Henderson JR. Simulation study of the disjoining pressure profile through a three-phase contact line. J Chem Phys 2010;132:84702. http://dx.doi.org/10.1063/1.3327840.
[32] Qian T, Wang X-P, Sheng P. Molecular hydrodynamics of the moving contact line in two-phase immiscible flows. Commun Comput Phys 2006;1:1–52.
[33] Shuttleworth R. The surface tension of solids. Proc Phys Soc Sect A 1950;63:444–57. http://dx.doi.org/10.1088/0370-1298/63/5/302.
[34] Ren W, Weiqing E. Boundary conditions for the moving contact line problem. Phys Fluids 2007;19:22101. http://dx.doi.org/10.1063/1.2646754.
[35] De Coninck J, Blake TD. Wetting and molecular dynamics simulations of simple liquids. Annu Rev Mat Res 2008;38:1–22. http://dx.doi.org/10.1146/annurev.matsci.38.060407.130339.
[36] Todd BD, Evans DJ, Daivis PJ. Pressure tensor for inhomogeneous fluids. Phys Rev E 1995;52:1627–38. http://dx.doi.org/10.1103/PhysRevE.52.1627.
[37] Irving JH, Kirkwood JG. The statistical mechanical theory of transport processes. IV. The equations of hydrodynamics. J Chem Phys 1950;18:817. http://dx.doi.org/10.1063/1.1747782.
[38] Marchand A, Das S, Snoeijer JH, Andreotti B. Capillary pressure and contact line force on a soft solid. Phys Rev Lett 2012;108. http://dx.doi.org/10.1103/PhysRevLett.108.094301.
[39] Navascués G, Berry MV. The statistical mechanics of wetting. Mol Phys 1977;34:649–64. http://dx.doi.org/10.1080/00268977700102021.